THREE-DIMENSIONAL NUMERICAL SIMULATION OF TURBULENT AIR FLOW IN VENTILATED ROOM, BY MEANS OF 2-EQUATION MODEL

Shinsuke KATO
Shuzo MURAKAMI

Institute of Industrial Science, University of Tokyo, Tokyo

SUMMARY

Turbulent recirculating flows in many types of ventilated rooms are numerically simulated three-dimensionally by means of k-ε 2-equation turbulence model. The results obtained from numerical simulation are compared with those given by model experiments concerned with air velocity and contaminant diffusion.

The correspondences between simulations and experiments are fairly good, so that it may be concluded that three-dimensional numerical simulation by means of k-ε 2-equation model can predict turbulent recirculating flows in a ventilated room with sufficient accuracy from the view point of engineering application.

NOTATION

C_D, C_1, C_2	empirical constants in turbulence model (*cf.* Table 2)
C	mean contaminant concentration
C_0	representative concentration defined by that of exhaust outlet
k	turbulence kinetic energy
k_0	boundary value for k of inflow
l	length scale of turbulence
l_0	boundary value for l of inflow
L_0	representative length defined by width of supply outlet
P	mean pressure
U, V, W	X, Y, Z components of velocity vector
U_i, U_j	component of velocity vector
U_0	representative velocity defined by inflow air velocity
ε	turbulence dissipation rate
ε_0	boundary value for ε of inflow
κ	von Karman constant, 0.4
ρ	fluid density
ν	molecular kinematic viscosity
ν_t	eddy kinematic viscosity
$\sigma_1, \sigma_2, \sigma_3$	turbulence Prandtl/Schmidt number of k, ε, C (*cf.* Table 2)

1. INTRODUCTION

The air flow in a ventilated room with a large air supply volume is usually highly turbulent and three dimensional. A typical example is the flow in a conventional type of clean room. The air flow distribution there should be controlled precisely because an undesirable air flow may diffuse airborne particles and may contaminate manufacturing processes. From this point of view, prediction of the air flow in clean rooms is one of the most important problems in the field of high technology engineering. Three-dimensional numerical simulation based on k-ε 2-equation turbulence model seems to be very promising

Table 1 Specifications of room models

Room type	Dimension of plan*1	Height of ceiling*1	Number of outlets	Number of inlets	Supply velocity*2	Remarks
Type 1	5×5	4.5	1	4	1.0	smallest room
Type 2	8×8	4.5	4	4	1.0	
Type 3	11×8	4.5	6	4	1.0	
Type 4	11×11	4.5	9	4	1.0	largest room
Type 5	11×11	4.5	4	4	1.0	
Type 6	11×11	4.5	1	4	1.0	

*1 Dimensionless value: all lengths have been made dimensionless by dividing by the width of supply outlet.
*2 Dimensionless value: all velocities have been made dimensionless by dividing by the inflow velocity.

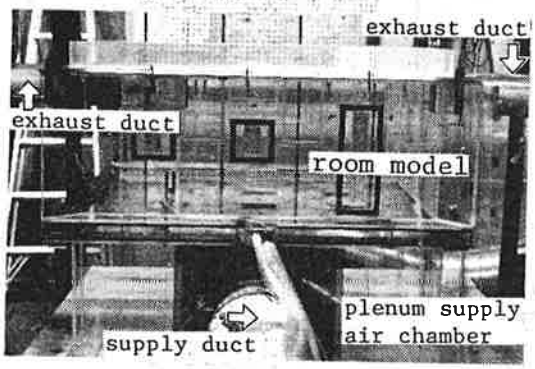

Photo 1 Model experiment

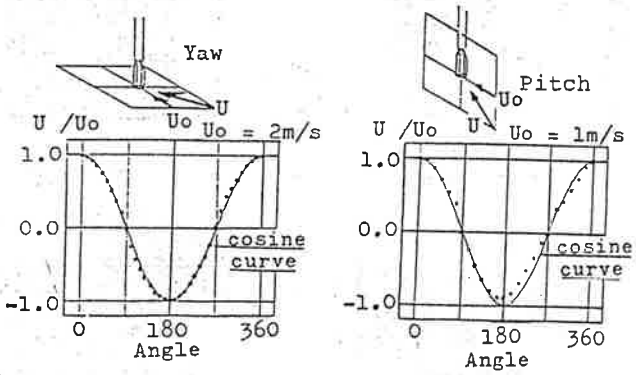

(a) Directivity (Yaw) (b) Directivity (Pitch)

Fig.1 Directivity of tandem type hot wire anemometer used

in answering that requirement.

The k-ε 2-equation model which was studied by Harlow and Nakayama (1967) and by Launder and Spalding (1972) has been widely applied in predicting many types of turbulent flow phenomena. Relatively few studies such as the works of Sakamoto and Matuo (1980) and Nomura, Murakami, Kato *et al.* (1980) have examined the accuracy of numerical simulation for three-dimensional elliptic turbulent flow phenomena, *i.e.* the three-dimensional recirculating flow in a ventilated room. Although air flow in a ventilated room is a most common phenomenon, there have been very few studies in which the distribution of the air velocities were measured in detail. Such detailed experiments may be used to examine the accuracy of the results of three-dimensional numerical simulation.

The main purpose of this paper is to verify the validity of the simulation. Therefore precise model experiments have been conducted and compared with numerical simulations.

2. MODEL ROOM USED FOR SIMULATION AND EXPERIMENT

Six types of room models are used in this study. In Table 1 the specifications of each room are presented. Fig.2 shows the geometry of each room model with the mesh dividing system used in numerical simulation.

In this study physical quantities are made dimensionless by dividing by representative quantities. Those quantities are the width of supply outlet L_0 and its bulk velocity U_0. The ceiling height of all types of room model is 4.5 in dimensionless value, which means that a jet from the ceiling outlet reaches the floor before it becomes a fully developed, self preserving turbulent jet because the distance between the floor and ceiling is only four and a half times

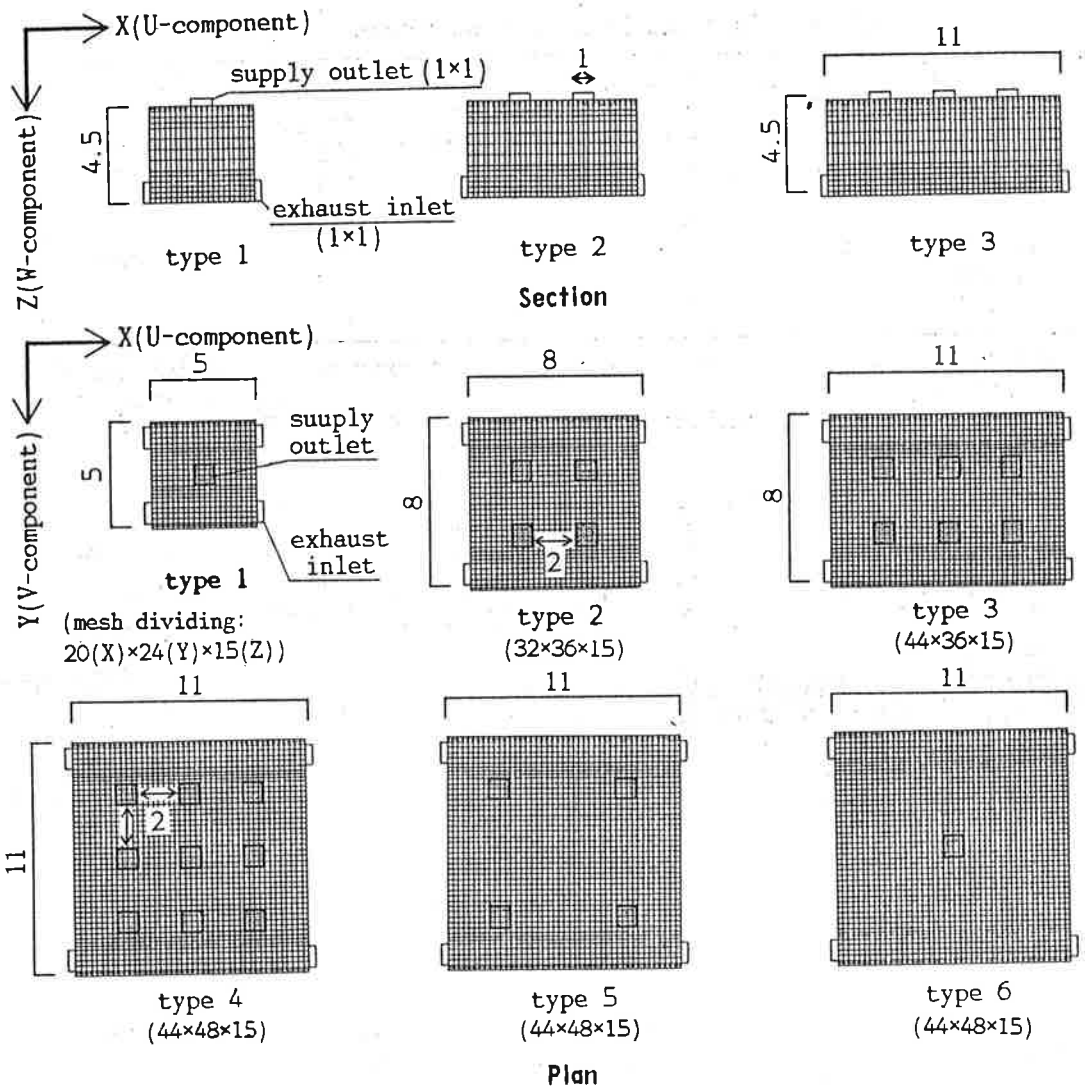

Fig.2 Model plans and mesh systems

the width of the outlet. The openings of the supply outlet and the exhaust inlet have the same shape.

3. MEASUREMENT OF AIR VELOCITY AND GAS CONCENTRATION IN ROOM MODEL

3.1 MODEL

The representative length, the width of supply outlet L_0, was set as 0.1m in the room models. The ceiling height of all types of room models is 0.45m. Hence these room models are made to a scale ratio of 1/6, for the ceiling height of full-scale rooms is usually 2.7m. The representative velocity, the velocity of the jet from the supply outlet U_0, was set at about 6m/s. The Reynolds number of the inflow jet U_0L_0/ν is about 4.2×10^4. The velocity of the jet from the supply outlet of full-scale conventional clean rooms is set at about 1m/s or so because of filter efficiency. Therefore the Reynolds number of the model experiment approximately corresponded to that of a full-scale clean room. The room models were placed upside down for convenience in measuring. Photo 1 shows the room model (the upper part) with the supply plenum chamber (the lower part) and the ducts connected to the exhaust inlet. Not only the rate of air volume but also the velocity distribution both at the outlets and at the inlets was carefully

Table 2 Model equations (2-equation of k-ε type)

$$\frac{\partial U_i}{\partial X_i} = 0 \tag{1}$$

$$\frac{\partial U_i}{\partial t} + \frac{\partial U_i U_j}{\partial X_j} = -\frac{\partial}{\partial X_i}\left\{\frac{P}{\rho} + \frac{2}{3}k\right\} + \frac{\partial}{\partial X_j}\left\{\nu_t\left\{\frac{\partial U_i}{\partial X_j} + \frac{\partial U_j}{\partial X_i}\right\}\right\} \tag{2}$$

$$\frac{\partial k}{\partial t} + \frac{\partial k U_j}{\partial X_j} = \frac{\partial}{\partial X_j}\left\{\frac{\nu_t}{\sigma_1}\frac{\partial k}{\partial X_j}\right\} + \nu_t S - \varepsilon \tag{3}$$

$$\frac{\partial \varepsilon}{\partial t} + \frac{\partial \varepsilon U_j}{\partial X_j} = \frac{\partial}{\partial X_j}\left\{\frac{\nu_t}{\sigma_2}\frac{\partial \varepsilon}{\partial X_j}\right\} + C_1\frac{\varepsilon}{k}\nu_t S - C_2\frac{k\varepsilon}{\nu_t} \tag{4}$$

$$\nu_t = k^{1/2} l = \left\{C_D \frac{k^2}{\varepsilon}\right\} \tag{5}$$

$$\frac{\partial C}{\partial t} + \frac{\partial C U_j}{\partial X_j} = \frac{\partial}{\partial X_j}\left\{\frac{\nu_t}{\sigma_3}\frac{\partial C}{\partial X_j}\right\} \tag{6}$$

here, $S = \left\{\frac{\partial U_i}{\partial X_j} + \frac{\partial U_j}{\partial X_i}\right\}\frac{\partial U_i}{\partial X_j}$, $\sigma_1 = 1.0$, $\sigma_2 = 1.3$, $\sigma_3 = 1.0$, $C_D = 0.09$, $C_1 = 1.59$, $C_2 = 0.18$

Table 3 Boundary Conditions (*cf.* 4.3)

(1) Supply Outlet boundary	$U_t = 0.0$, $U_n = U_{out}$, $k = 0.05$, $l = 0.75$, $C = 0.0$ suffix t: tangential component n: normal component U_{out} = Supply outlet velocity, $U_{out} = 1.0$
(2) Exhaust Inlet boundary	$U_t = 0.0$, $U_n = U_{in}$, $\partial k/\partial z = 0.0$, $\partial \varepsilon/\partial z = 0.0$, $\partial C/\partial z = 0.0$ U_{in} = Exhaust inlet velocity, *e.g.* type 1: $U_{in} = 0.25$
(3) Wall boundary	$(\partial U_t/\partial z)_{z=0} = m\,(U_t)_{z=h}/h$, $U_n = 0.0$, $\partial k/\partial z = 0.0$, $\partial C/\partial z = 0.0$ $(\varepsilon)_{z=h} = [C_D\, k_{z=h}^{3/2}]/[C_D^{1/4}\kappa h]$ h = Length from the wall surface to the center of the adjacent cell m = 1/7 , power law of profile $U_t(z) \propto z^m$ is assumed here. κ = von Karman constant, z: coordinate normal to the wall

adjusted so that the degree of scatter in the measured values falls within ±7% of the respective average values.

3.2 MEASUREMENT OF AIR VELOCITY AND GAS CONCENTRATION

Air velocity was measured by means of a tandem type, parallel hot-wire anemometer which can discern the vector components of turbulent flow. Fig.1 shows the directivity of the anemometer used. The calibration curve closely corresponds to cosine curve.

The mechanism of passive scalar diffusion is investigated by means of a tracer gas diffusion experiment. Ethene C_2H_4 is used for the tracer and its concentration is measured by means of a F.I.D. gas chromatography.

4. NUMERICAL SIMULATION

4.1 MODEL EQUATION AND NUMERICAL METHOD

Model equations (k-ε 2-equation turbulence model) are given in Table 2. Equation (6) is a transport equation of passive contaminant. Source term in (6) is omitted as its value is always zero except at the source point. A staggered mesh system is adopted. The definition points of the variables are the same as those in the usual Marker-And-Cell(MAC) method [Harlow and Welch (1965)]. Velocity components are defined on the center of the cell surfaces and scalar quantities are set in the center of the cell. Centered difference scheme is

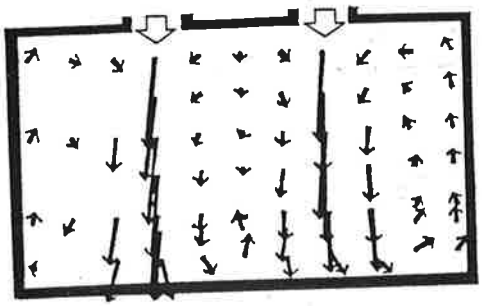

(a) Velocity vectors(U+W)

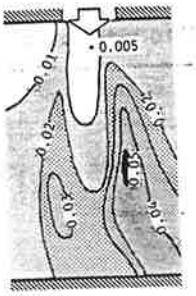

(b) Turbulence energy(k) (dimensionless)

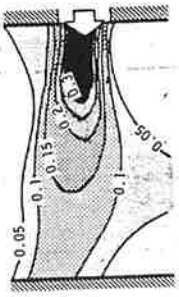

(c) Turbulent length scale(l^*) (dimensionless)

Here l^* is estimated from the experiment with the following procedure:

$$T_i = \int R_i(\tau)\,d\tau$$

$$T_A = \frac{1}{3}(T_X + T_Y + T_Z)$$

$$L = \sqrt{U^2+V^2+W^2} * T_A$$

$$l^* = C_D^{1/4} * L$$

Fig.3 Results of model experiment in case of type 2 (vertical section including supply outlets)

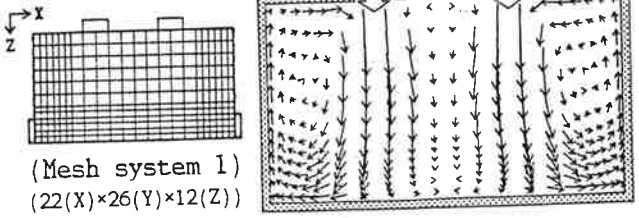

(Mesh system 1)
(22(X)×26(Y)×12(Z))

(a) Velocity vectors obtained from mesh system 1, in which four meshes are set between two outlets and 2×2 cells on the outlet plane

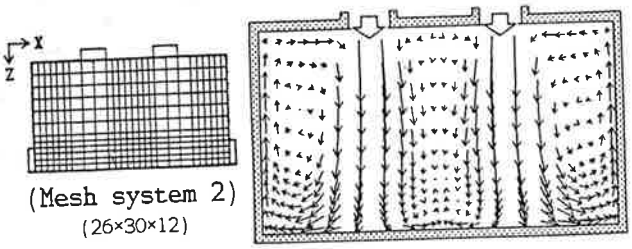

(Mesh system 2)
(26×30×12)

(b) Velocity vectors obtained from mesh system 2, in which eight meshes are set between two outlets and 2×2 cells on the outlet plane

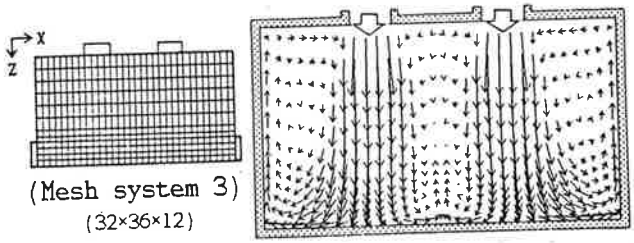

(Mesh system 3)
(32×36×12)

(c) Velocity vectors obtained from mesh system 3, in which eight meshes are set between two outlets and 4×4 cells on the outlet plane

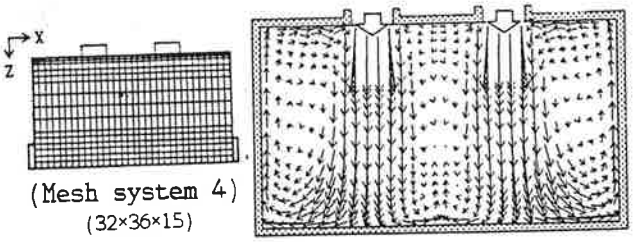

(Mesh system 4)
(32×36×15)

(d) Velocity vectors obtained from mesh system 4, which adopts finer meshes near ceiling plane

Illustrated plane

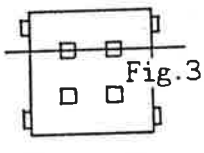

Fig.3,4,5

Plan of type 2

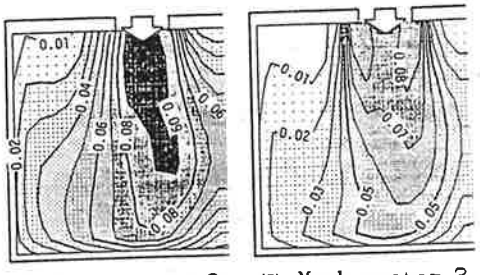

(1) Mesh system 2 (2) Mesh system 3

(e)Turbulence energy(k)

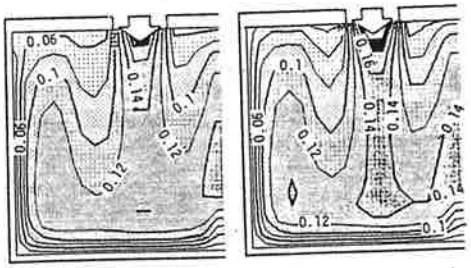

(1) Mesh system 3 (2) Mesh system 4

(f)Turbulent length scale(l)

Fig.4 Comparisons of simulations based on different mesh systems

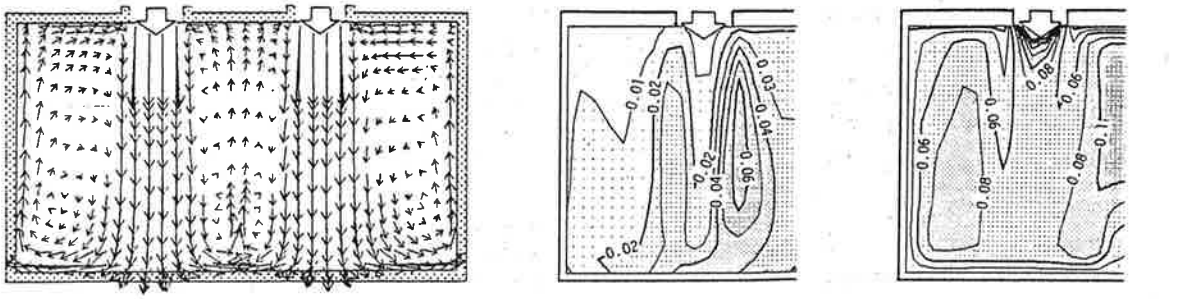

(a) Velocity vectors(U+W) (b) Turbulence energy(k) (c) Turbulent length scale(l)

Fig.5 Simulation using measured values of k and l as the inflow boundary condition

adopted for both the convective terms and other terms. Up-wind difference scheme is partially adopted only near the exhaust inlet in order to remove the spatial oscillation due to the numerical instability. For discretization in time, Adams-Bashforth method is used. Numerical integration is conducted following the ABMAC method, a simultaneous iteration method for pressures and velocities and stationary solutions are obtained [Viecelli (1971), Hirts and Cook (1972)].

4.2 MESH SYSTEM

The mesh systems used are shown in Fig.2. In order to examine the influence of the mesh resolution upon the result of the simulation, preliminary numerical simulations based on various coarse mesh systems were conducted and the results were compared with the experimental data. Fig.3 shows the results of a model experiment of type 2, and Fig.4 shows the results of preliminary simulations which used the boundary condition given in Table 3. As shown in Fig.4(a) and Fig.4(b), when the mesh resolution was coarse between the outlets, a rising stream between the jets near the floor was not reproduced. As shown in Fig.4(b), Fig.4(c) and Fig.4(e), when the mesh resolution was coarse around the outlet jet, the distribution of turbulence energy k at the mixing layer of the jet was not well reproduced although the velocity distribution was well simulated. In the simulations with coarse mesh(Fig.4(e)-(1)), the distribution of turbulence energy k had a uniformly high value under the outlet. But in the simulation with finer mesh(Fig.4(e)-(2)), the distribution of the turbulent energy k under the supply outlet had a low value at the center of the jet and had a high value around the outer edge of the jet where the mixing layer might exist. As shown in Fig.4(c), Fig.4(d) and Fig.4(f), when the resolution was coarse near the ceiling, the distribution of scale of turbulence "l" around the jet was not well reproduced though its influence on the mean velocity was very slight also.

From the above mentioned analyses, the mesh systems shown Fig.2 were adopted in this study.

4.3 BOUNDARY CONDITION

The boundary conditions for rigid walls are assumed as follows. They are summed up also in Table 3.

1) Velocity component normal to the wall is zero at the wall. The profile of tangential air velocity near the wall obeys the distribution expressed as $U(z) \propto z^m, m=1/7$. 2)The gradient of turbulence energy k normal to the wall is zero, namely $\partial k/\partial z=0$. 3) The length scale of turbulence l is proportional to the distance from the wall, namely $l\ (z)=C_D^{1/4}\kappa z$. (Here, z denotes the coordinate normal to the wall.)

The boundary conditions for inflows are given as follows.

1) Uniform velocity distribution is assumed over supply outlet. 2) Uniform k and

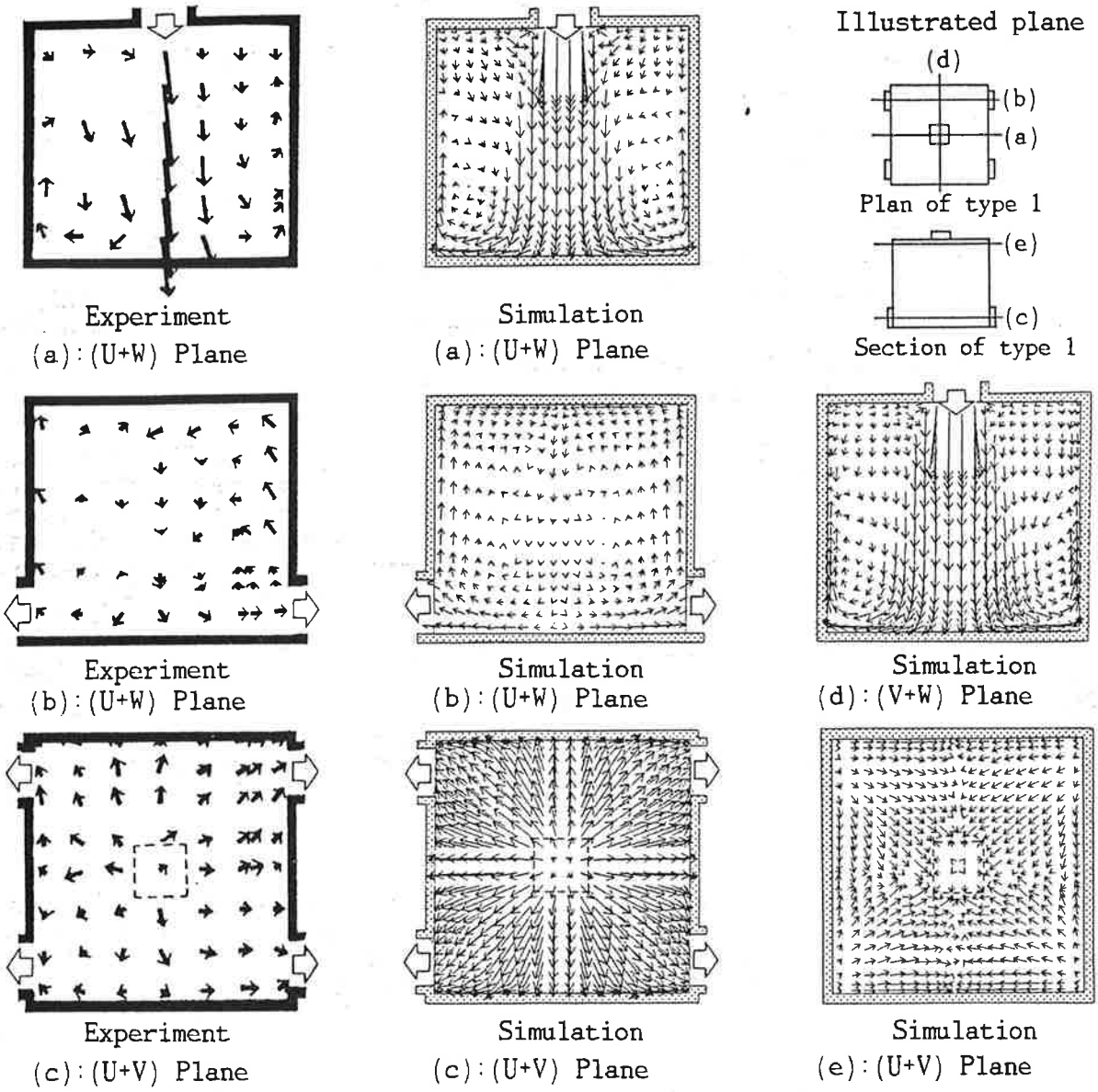

(vector length of supply outlet velocity: ⟶)

Fig.6 Comparison of velocity vectors in type 1 room model

ε distributions are also assumed over supply outlet. The values k_0, ε_0 used in these simulations were chosen after considering the results of many trial computations. They are larger than those given by the measurements. The velocity distribution of the simulation which adopted the boundary condition for k_0, ε_0 according to the values obtained from the measurement (k_0=0.005, l_0 =0.33, $\varepsilon_0=C_D k_0^{3/2}/l_0$), was obviously different from that given by the experiment, as is shown in Fig.5(a) and Fig.3(a). Thus the simulation with the tuned values of k_0=0.05 and l_0 =0.75 corresponds fairly well to the experiment, as is shown in Fig.4(d) and Fig.3(a).

The boundary conditions for outflows are assumed as follows.
1) Uniform velocity distribution is assumed over exhaust inlet. 2) The gradient of k, ε ,C normal to the exhaust inlet is zero.

5. COMPARISON BETWEEN NUMERICAL SIMULATION AND EXPERIMENTAL RESULTS FOR AIR VELOCITY

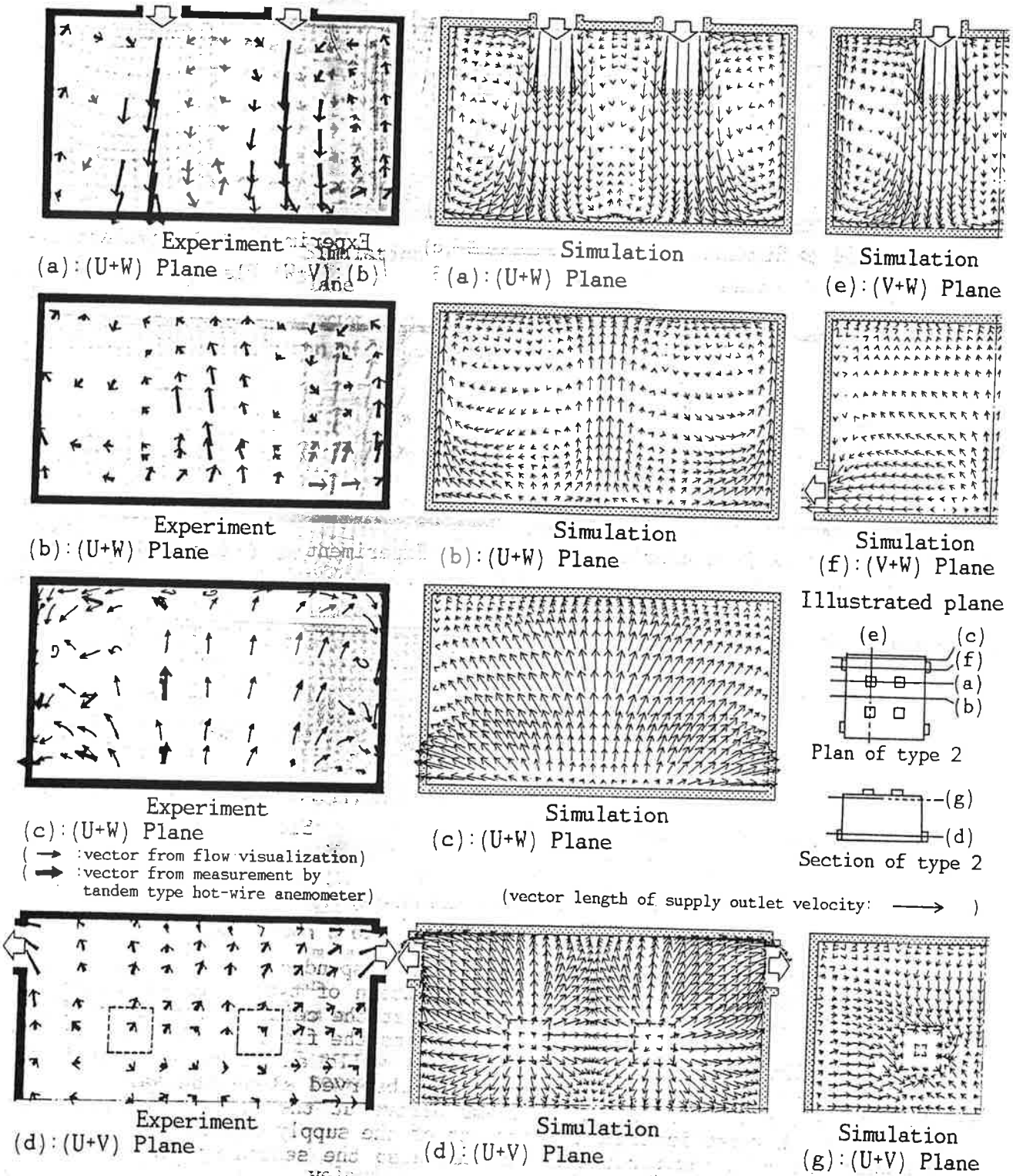

Fig.7 Comparison of velocity vectors in type 2 room model

5.1 TYPE 1

The distributions of velocity vectors in the several sectional planes are compared in Fig.6. Although the velocity vectors in planes (d) and (e) are obtained only from simulation, they are presented here so as to help

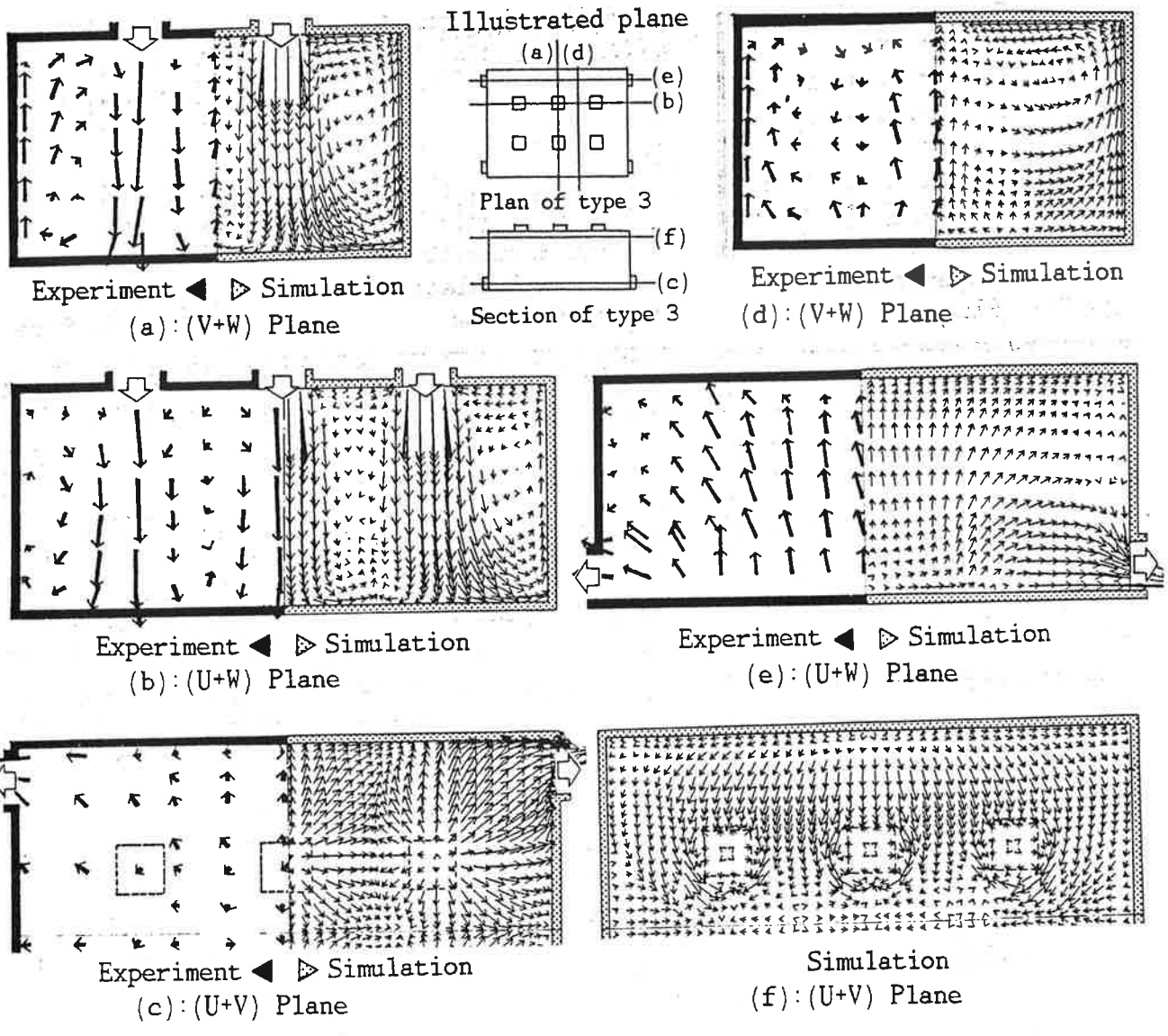

Fig.8 Comparison of velocity vectors in type 3 room model

comprehension of the entire flow field. The correspondence of the simulations with the experiment is good. The mean flow pattern of type 1 is summarized as follows. 1) The air jet from the supply outlet at the ceiling reaches the floor without velocity decrease. 2) The jet stream hits the floor and diverges toward the wall. 3) The diverged streams reach the walls and turn up toward the ceiling. Thin and strong rising streams are observed along the walls to the ceiling. 4) After the rising wall-streams arrive at the ceiling and converge toward center, they are induced into the jet of the supply outlet.

Not only the main recirculating flow but also the secondary flows are well reproduced by this numerical simulation.

5.2 TYPE 2

The distributions of velocity vectors in the several sectional planes are compared in Fig.7. The distributions of velocity vectors in planes (e), (f), and (g) are not measured in the experiment. Some points of the flow pattern of type 2 are similar to those of type 1. It may be reasonable modelling to regard the flow pattern of type 2 as a combination of the four flow patterns of type 1. In

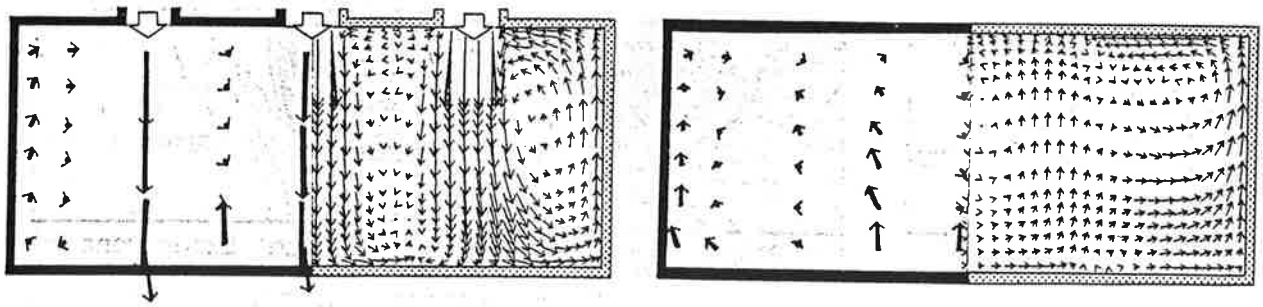

Fig.9 Comparison of velocity vectors in type 4 room model

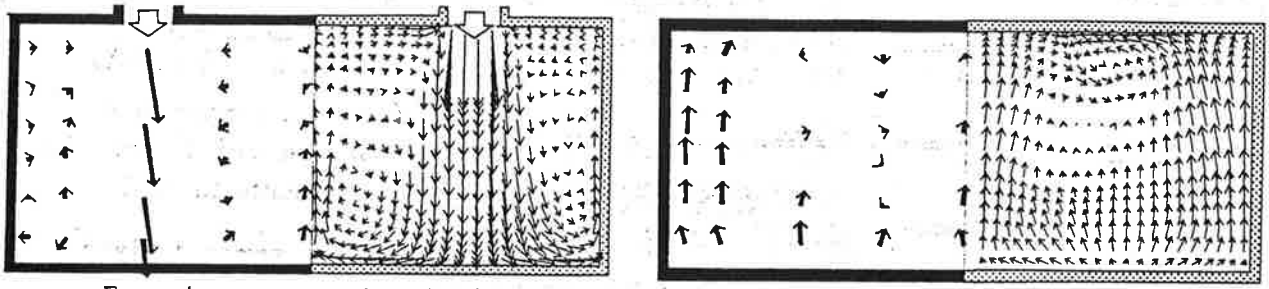

Fig.10 Comparison of velocity vectors in type 5 room model

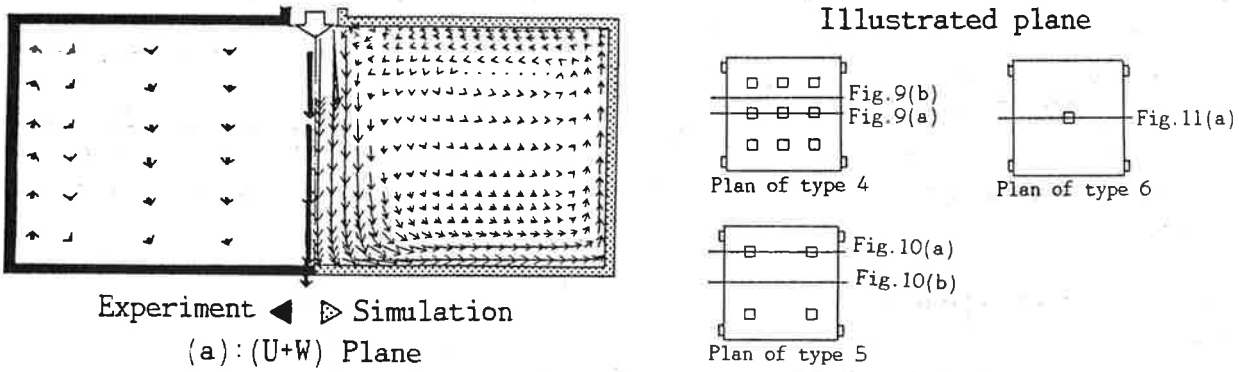

Fig.11 Comparison of velocity vectors in type 6 room model

the type 2 model room, not only the main recirculating flow but also the secondary flows are well reproduced by numerical simulation.

5.3 TYPE 3

The distributions of velocity vectors in the several sectional planes are compared in Fig.8. Generally the correspondences between the numerical simulation and the experiment are excellent. But there are slight differences in the (a) sectional plane. In that plane of the experiment, the rising stream between two jets attacks the ceiling but at the same position in the simulation the rising stream does not reach the ceiling. The rising streams between the jets are extreamly sensitive to the inflow air volume rate of each outlet. On the other hand, the rate of inflow air volume is very difficult to control exactly in the experiment. It may therefore be concluded that these differences

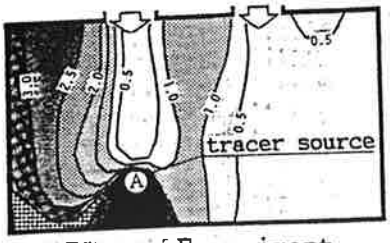

(a) Plane; Experiment

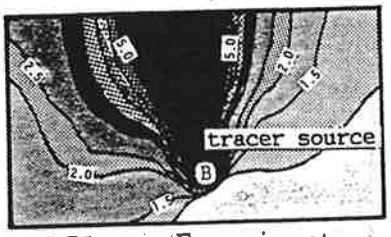

(c) Plane; Experiment

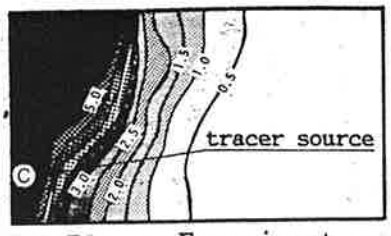

(c) Plane; Experiment

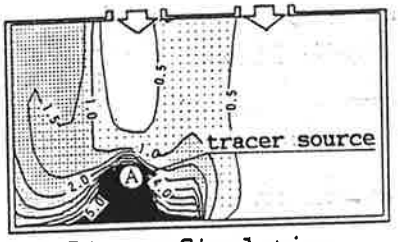

(a) Plane; Simulation

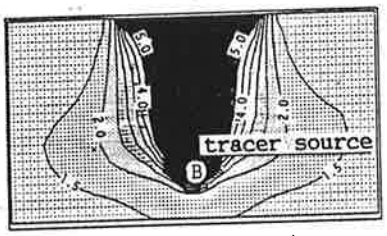

(c) Plane; Simulation

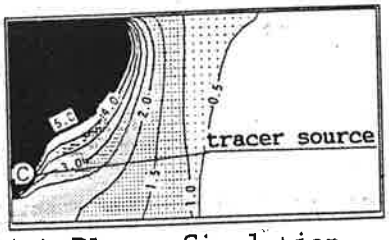

(c) Plane; Simulation

Fig.14 Comparison of contaminant distribution, source:point C

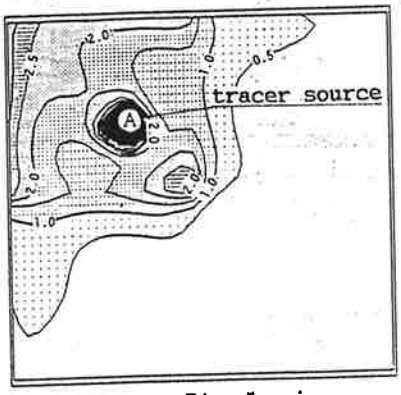

(b) Plane; Simulation

Fig.12 Comparison of contaminant distribution, source:point A

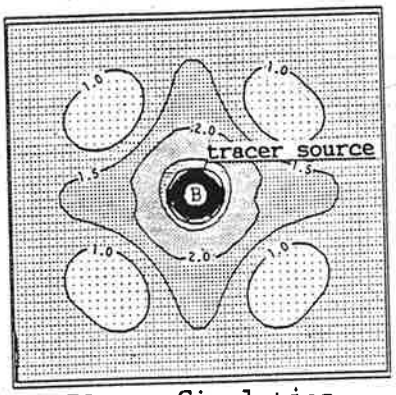

(b) Plane; Simulation

Fig.13 Comparison of contaminant distribution, source:point B

Illustrated plane

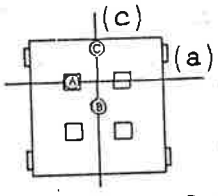

Plan of type 2 Section of type 2

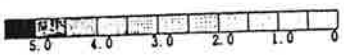

Dimensionless concentration

between the simulation and the experiment may not be due only to inaccuracy in the simulation.

5.4 TYPE 4, TYPE 5 AND TYPE 6

Fig.9 shows a comparison of velocity vectors in the type 4 room model. As in the other types of room model, not only the main recirculating flow but also the small vortexes are well reproduced by the numerical simulation. Fig.10 and Fig.11 show comparisons of velocity vectors in the type 5 and type 6 room models respectively. The correspondences between the numerical simulations and the experiments are quite close.

6. COMPARISON BETWEEN NUMERICAL PREDICTIONS AND EXPERIMENTAL RESULTS FOR CONTAMINATION CONCENTRATION

The distributions of passive scalar contaminant (airborne particles or gas contaminant) of simulations and experiments are compared. For these comparisons the type 2 room model was used. Three comparisons are conducted with respect to the three different positions of the tracer source. The contaminant

concentrations of both the experiments and the simulations are normalized by the average value of the exhaust outflow concentration. Fig.12 shows a comparison of distribution of contaminant concentration in the case where tracer source is located at point A. The distribution in section (b) (horizontal plane) is presented only for numerical simulation. The distribution given by the numerical simulation corresponds well to the experimental data. Although the contour lines of concentration are not exactly the same, the main characteristics of contaminant diffusion are well reproduced, for example the shape of the high concentration region under the tracer source, the low concentration region under the supply outlet, and the low concentration part of the opposite side where no tracer source exists.

Fig.13 and Fig.14 show comparisons of distributions of contaminant concentration in the case where the tracer source is located at point B and at point C respectively. As the contaminant is transported mainly by the main air flow, the high concentration region spreads from the tracer source along the main flow direction. While contour lines of concentration of the simulations do not correspond so well as those in Fig.12, the main characteristics of the contaminant diffusion are generally the same.

From the view point of engineering application, it may be concluded that numerical simulation can well predict contaminant diffusion.

7. CONCLUSION

It is confirmed that numerical simulation of the three-dimensional turbulent recirculating flow in a ventilated room by means of k-ε model corresponds well to experimental results.

There still remain several problems in numerical simulation, such as the boundary conditions of inflow and others; more study must be conducted to clarify these problems.

ACKNOWLEDGMENTS

The authors wish to thank the generous co-operation of Y. Suyama, Joint Researcher of IIS,University of Tokyo, Hazama-gumi Co.Ltd. and S. Nagano, Research Student of IIS,University of Tokyo, Fujita Corporation.

REFERENCES

Launder,B.E. and Spalding,D.B.:Mathematical models of turbulence, Academic Press, London and New York, 1972.

Harlow,F.H. and Welch,J.E. "Numerical Calculation of Time-Depended Viscous Incompressible Flow of Fluid with Free Surface" Phys.Fluids vol.8, 2182～2189, 1965.

Harlow,F.H. and Nakayama,P.I. "Turbulence Transport Equations" Phys.Fluids vol.10, 2323～2332, 1967.

Hirt,C.W. and Cook,J.L. "Calculating Three-Dimensional Flows around Structures and over Rough Terrain" J.Comput.Phys vol.10, 324～340, 1972.

Nomura,T., Murakami,S., Kato,S., and Sato,M. "Correspondence of the Three-Dimensional Numerical Analysis of Turbulence Flow to Model Experiment" Transactions of Architectural Institute of Japan No.298, 69～80, 1980.

Murakami,S. and Kato,S. "Correspondence of Numerical Simulation of Room Air Flow to Model Experiment" SEISAN-KENKYU, IIS, University of Tokyo, vol.36, 532～535, 1985.

Sakamoto,Y. and Matuo,Y. "Numerical predictions of three-dimensional flow in a ventilated room using turbulence models" Appl.Math.Modelling, vol.4, 67～72, 1980.

Viecelli,J.A. "A Computing Method for Incompressible Flows Bounded by Moving Walls" J.Comput.Phys, vol.8, 119～143, 1971